


Trapping Force of Acoustical Bessel Beams on a Sphere and Stable Tractor Beams

Xu-Dong Fan and Likun Zhang*

National Center for Physical Acoustics and Department of Physics and Astronomy, University of Mississippi, University, Mississippi 38677, USA

 (Received 9 August 2018; revised manuscript received 15 November 2018; published 28 January 2019)

We seek stable tractor beams that not only axially pull objects but also transversely trap the object. Transverse force acting on a spherical particle centered on the axis of acoustic Bessel beams is examined using the Gor'kov potential and partial wave expansion. The results suggest flexibility of trapping both relatively dense and stiff particles and relatively light and soft particles at the pressure maximum of the axisymmetric Bessel beam in the Rayleigh regime. This trapping is more flexible than trapping by standing waves and focused beams used in acoustic tweezers. The flexibility is interpreted by the contribution of axial velocity to the force potential and by momentum projection. We then reveal parameters (paraxiality, density ratio, and bulk modulus ratio) for simultaneous trapping and pulling of an elastic object and droplet in and beyond the Rayleigh regime. The results reveal the capability and conditions to simultaneously trap and pull a Rayleigh particle even in the situation when losses are accounted for. Our study guides designs of stable tractor beams and drives development of acoustic tweezers.

DOI: [10.1103/PhysRevApplied.11.014055](https://doi.org/10.1103/PhysRevApplied.11.014055)

I. INTRODUCTION

Focused laser beams have been used as “optical tweezers” to trap particles by gradient forces [1] and applications of such beams in biological sciences have been found. On the other hand, nondiffracting beams have been found to produce nonconservative radiation forces that can pull particles against the propagation direction of the beam (like a “tractor beam”), first reported in acoustics [2–4] and later in optics [5–8], which extends the flexibility of particle manipulations. The pulling can be interpreted in the framework of momentum conservation [3,4,6]. In optics, the simultaneous pulling by nonconservative forces and trapping by a gradient force have been reported [9–11]. In acoustics, a transversely stable acoustic pulling force using two intersecting plane waves was analyzed in Ref. [12] and experimentally realized in Ref. [13] using a two-dimensional source array for a large triangular object. For acoustic Bessel beams, the transverse stability may be evaluated using the numerical approaches discussed in Refs. [14–16]. A fully analytical expression for the transverse force in terms of the partial wave expansion only became available until recently in Ref. [17], which enables a systematic examination of the trapping. This paper addresses conditions and parameters for simultaneous pulling and trapping of a spherical particle in and

beyond the Rayleigh regime and for practical selections of parameters when absorption is accounted for.

When considering the illumination of acoustical Bessel beams on a Rayleigh particle, where the contributions are from monopole and dipolar fields, the pulling appears to be limited by two facts: (i) the axisymmetric beam has to be used because the scattering asymmetry desired by the pulling force relies on the superposition of the monopole and dipolar fields [3,4] (while the vortex beams would otherwise suppress the monopole field [3,18,19]) and (ii) the negative force can be made positive by the absorption contribution when the particle is sufficiently small [3,20,21]. With regards to trapping, acoustical trapping of a small particle in the Rayleigh regime has been considered in the concept of force potential since a seminal work by Gor'kov [22]. Acoustic traps using *standing* waves have become an important tool for acoustic levitation (e.g., [23]) and particle separation (e.g., [24]). Acoustic traps by focused ultrasound beams are being developed to act as an acoustic counterpart to optical traps for applications in biomedical and material engineering [25–34]. In the Rayleigh regime, an axisymmetric focused beam can transversely trap a relatively light and soft particle (like droplets) to the central pressure maximum [26], but a relatively dense and stiff particle would be repelled away from the beam axis [35]. Transverse trapping of relatively dense and stiff particles (like elastic objects) has to rely on using focused vortex beams that have a central pressure null along the core [29–31]. These trapping behaviors

*zhang@olemiss.edu

appear to be consistent with trapping by plane standing waves [22] or Bessel-function standing waves [36], in the manner that relatively dense and stiff particles are likely trapped to the pressure minimum (node), while relatively light or soft particles are likely trapped to the pressure maximum (antinode). However, transverse trapping by acoustic Bessel beams can have behaviors very different from trapping by standing waves and focused beams, as we demonstrate and explain.

In this present work, our systematic examinations of trapping by acoustic Bessel beams allow us to gain insight into some unusual and unique trapping behaviors beyond trapping by standing waves and focused beams and, in turn, we report flexibility of trapping elastic particles by axisymmetric beams and conditions for simultaneous trapping and pulling of a small particle. We consider a particle centered on the central core of both axisymmetric beams (pressure maximum) and vortex beams (pressure minimum) (Fig. 1), described by arbitrary-order Bessel beams propagating along a z axis with the pressure field $\text{Re}[p(\mathbf{r}, t)]$ (Re denotes the real part) given by

$$p(\mathbf{r}, t) = p_0 J_l(\mu\rho) \exp(ikz + il\phi - i\omega t), \quad (1)$$

where p_0 is a real-valued amplitude; J_l is a Bessel function with a topological charge of l ; $\mathbf{r}(\rho, \phi, z)$ is the field point in cylindrical coordinates; and the transverse wavenumber μ and axial wavenumber κ are related to the total wavenumber $k = \sqrt{\mu^2 + \kappa^2} = \omega/c_0$ (c_0 is sound speed in

the surrounding media) through a paraxiality parameter β with $\mu = k \sin \beta$ and $\kappa = k \cos \beta$.

II. TRAPPING OF A RIGID SPHERE

For the transverse force $F_\rho = \pi a^2 (I_0/c_0) Y_\rho$ exerted on a spherical particle of radius a [with $I_0 = p_0^2/(2\rho_0 c_0)$ being the acoustic intensity and ρ_0 the density of the surrounding media], the dimensionless transverse force Y_ρ as a function of the transverse location R of the sphere off the beam axis is given by Eq. (16) in Ref. [17]:

$$Y_\rho(R) = \sum_{m=-\infty}^{\infty} K_m^+ B_m, \quad (2)$$

$$K_m^+ = J_{l-m}(\mu R) J_{l-m-1}(\mu R) - J_{l+m}(\mu R) J_{l+m+1}(\mu R),$$

$$B_m = \frac{1}{(ka)^2} \sum_{n=|m|}^{\infty} \frac{(n-m)!}{(n+m)!} P_n^m(b) P_{n+1}^{m+1}(b) \text{Im}(s_n^* s_{n+1}),$$

where $b = \cos \beta$, Im represents the imaginary part, and the scattering functions s_n [37] are determined by boundary conditions on the particle surface (see the Appendix; $|s_n| = 1$ in the ideal case of no absorption). Note that $K_m^+ = 0$ when $\mu R = 0$. The transverse force as a function of the object location R calculated for a dense and rigid particle ($ka = 0.05$ and $\beta = 15^\circ$) is shown in Fig. 1. From the results, we find that the particle is trapped to the axis

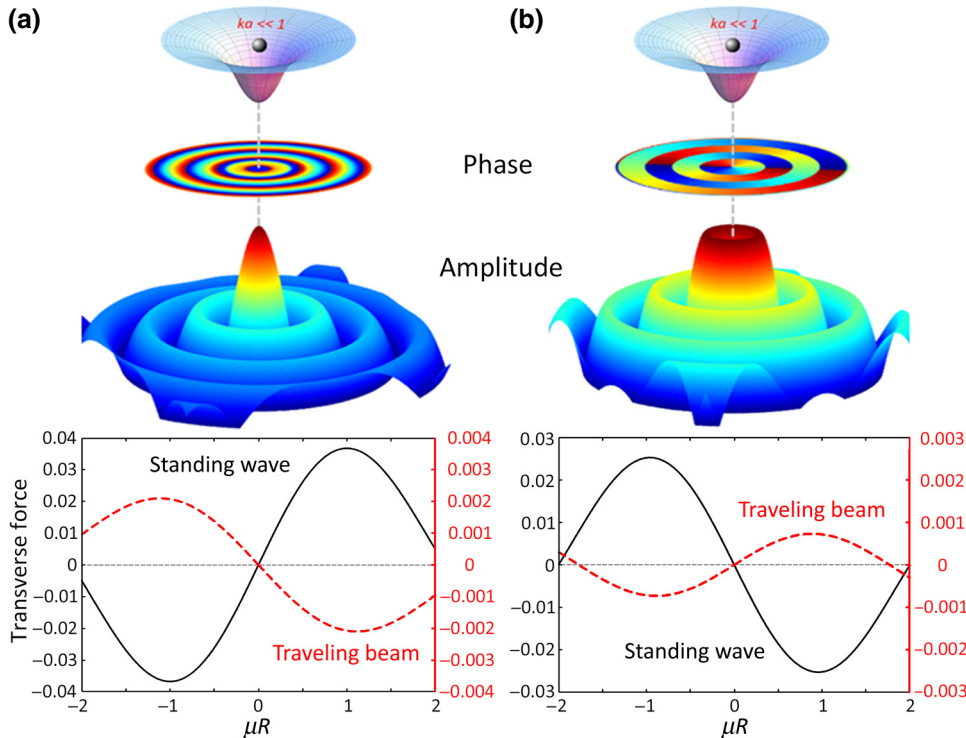


FIG. 1. A fixed rigid sphere is laterally trapped at the central core of the pressure maximum of axisymmetric beams [left in panel (a)] and repelled from the pressure minimum of vortex beams [right in panel (b)] for a Rayleigh particle of a radius a ($ka = 0.05$ with k being wavenumber), as shown by the dimensionless transverse force as a function of the object location R . The results are for traveling beams of paraxiality parameter $\beta = 15^\circ$ (red dashed lines) with a comparison of standing waves of $\beta = 90^\circ$ (black solid lines). The fields are given by Eq. (1) with the topological charge $l = 0$ and 1, respectively.

of the axisymmetric beam and repelled away from the core of the vortex beam (red dashed lines), in contrast to the trapping behaviors by standing waves (black solid lines).

We understand the contrast behaviors by the contribution of the velocity component along the propagation direction to the force potential. In the Rayleigh regime, the transverse force is given by $F_\rho = -\partial U/\partial \rho$, where the gradient is along the transverse direction only, but the force potential U depends on velocity in all three directions [22],

$$U = (\pi a^3/3)[f_1 |p|^2/(\rho_0 c_0^2) - (3/2)f_2 \rho_0 |\mathbf{v}|^2], \quad (3)$$

in which the monopole and dipole factors,

$$f_1 = 1 - 1/\kappa, \quad f_2 = 2(\lambda - 1)/(1 + 2\lambda), \quad (4)$$

depend on the mass density ratio and bulk modulus ratio of the particle to the surrounding media:

$$\lambda = \rho/\rho_0, \quad \kappa = K/K_0. \quad (5)$$

For the axisymmetric beam [Fig. 2(a)], it is true that the transverse velocity has a central minimum coinciding with the pressure maximum, like planar standing waves, leading to a maximum of the Gor'kov potential for a relatively stiff and dense particle. However, the axial velocity component instead has a central maximum coinciding with the pressure maximum. As a result, it is possible to have a minimum potential for a stiff and dense particle ($f_{1,2} > 0$) or even for the extreme case of a rigid particle ($f_1 = 1$), as long as the particle is dense enough (large f_2). The minimum potential for a rigid particle of heavy mass ($f_{1,2} = 1$)

centered on the axisymmetric beam is shown in Fig. 2(a). Similarly, for the vortex beam [Fig. 2(b)], the transverse and azimuthal velocity has a central maximum coinciding with the pressure minimum, like planar standing waves, leading it to trap a relatively dense and stiff particle by the minimum of the Gor'kov potential. However, the axial velocity component instead has a central minimum coinciding with the pressure minimum. As a result, a stiff and dense particle could be repelled from the pressure null of vortex beams due to the maximum potential as shown in Fig. 2(b).

Given the projection of wave vectors associated with the paraxiality parameter β , the transverse velocity is proportional to $\sin \beta$ while the axial velocity is proportional to $\cos \beta$:

$$v_\rho \propto \sin \beta, \quad v_z \propto \cos \beta. \quad (6)$$

As such, reducing the paraxiality parameter β would reduce the transverse velocity and enhance the axial velocity. Consequently, the trapping would be reversed when the β is reduced to be smaller than a critical value. The reversal occurs only when the density contrast is large enough [see Eq. (3)].

III. VARIATION OF TRAPPING WITH BEAM AND MATERIAL PARAMETERS

The above predictions of variation of the trapping with beam and material parameters are exactly shown in Fig. 3 by the transverse gradient of the transverse force:

$$\text{Slope} = dY_\rho(R)/d(\mu R). \quad (7)$$

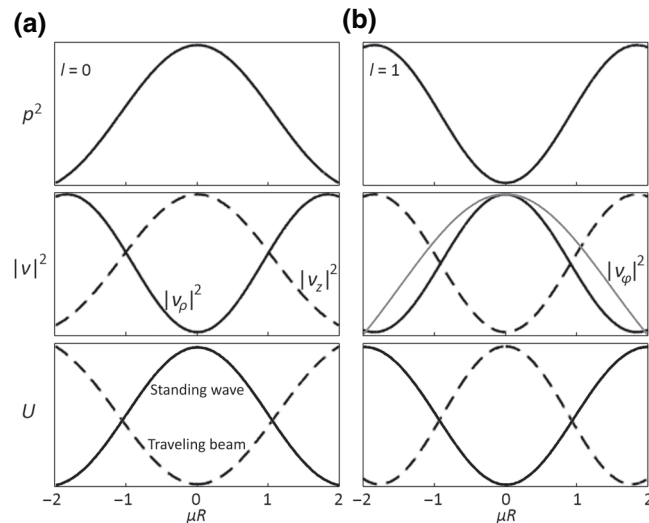


FIG. 2. Contribution of pressure (top panels) and three components of velocity (center panels) to the potential (bottom panels) for (a) axisymmetric and (b) vortex beams. The reversal of the potential is due to the presence of axial velocity (dashed lines). Arbitrary units and normalization are used here.

The results are for the slope as a function of the paraxiality parameter β calculated from Eq. (2) with $ka = 0.05$ for four different contrasts of density and bulk modulus. At the nonpropagating limit $\beta = 90^\circ$, the results are in agreement with trapping by plane standing waves or trapping by Bessel-function fields: the light or soft particles are trapped at the pressure antinode (local maximum) of axisymmetric waves [Figs. 3(a) and 3(c)], while dense and stiff particles are trapped at the pressure node (local minimum) of vortex waves [Figs. 3(b) and 3(d)]. When we reduce the β to change to a traveling beam, the results show exactly that the trapping is preserved when the density contrast is relatively small [(a) and (b)] and reversed when the density contrast is relatively large [(c) and (d)]. Meanwhile, the transition difference of β between $l = 0$ and $l = 1$ leads to repelling [see (c)] or trapping [see (d)] by both axisymmetric and vortex beams at β values between the two transitions, while it is generally true that the particles trapped by one beam are repelled by another one.

We characterize the transverse force in terms of a beam-parameter-dependent acoustic contrast factor Φ_l and the

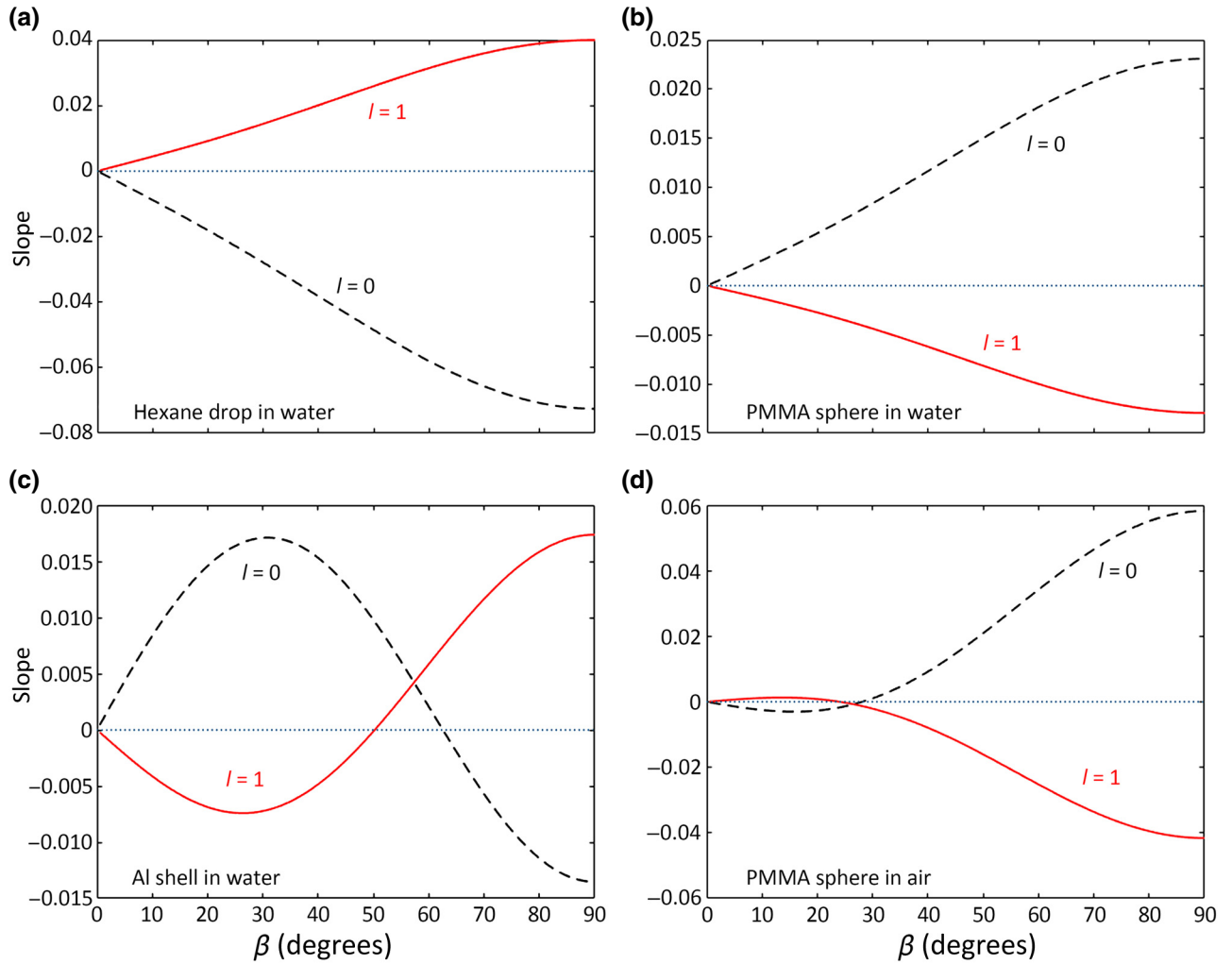


FIG. 3. When varying the paraxiality parameter β , the trapping is (a),(b) preserved for a small contrast of density or (c),(d) reversed for a large contrast of density, as denoted by the sign of the slope [see Eq. (7)]. The inner-to-outer radius ratio of the aluminum shell in (c) is 0.96; see the material parameters in Table I.

dimensionless transverse location μR explicitly:

$$Y_\rho = 2ka \sin \beta \Phi_l \times \mu R + O[(\mu R)^2], \quad (8)$$

where $\sin \beta$ accounts for the momentum projection to the transverse direction. For $l = 0$ and 1 beams, we obtain

$$\Phi_l = \pm 2^{-l} \left[\frac{1}{3} f_1 + \left(\frac{3+l}{4} \sin^2 \beta - \frac{1}{2} \right) f_2 \right], \quad (9)$$

which follows from (a) the Gor'kov potential Eq. (3), where the velocity is $\mathbf{v} = \nabla p / (i\omega\rho_0)$, with the pressure p given by Eq. (1), or (b) the partial wave expansion Eq. (2), where only the monopole and dipole terms are kept and the partial wave coefficients at the small ka approximation are

used [21]:

$$s_0 = 1 - i(2/3)(ka)^3 f_1 - (2/9)(ka)^6 f_1^2, \quad (10a)$$

$$s_1 = 1 + i(1/3)(ka)^3 f_2 - (1/18)(ka)^6 f_2^2. \quad (10b)$$

TABLE I. Acoustic properties of materials in Fig. 3. PMMA represents for poly methyl methacrylate. The density 311 kg/m^3 is the effective density of the aluminum shell calculated with the inner-to-outer radius ratio $b/a = 0.96$.

Materials	Mass density ρ (kg/m ³)	Longitude wave speed c_L (m/s)	Transverse wave speed c_T (m/s)
Air	1.21	343	
Hexane	656	1078	
Water	1000	1500	
PMMA	1190	2690	1340
Aluminum	2700 (311)	6420	3040

The small μR approximation is applied, $J_m(\mu R) \approx (\mu R/2)^m/m!$ [with m being a non-negative integer and $J_m(x) = (-1)^m J_{|m|}(x)$ for a negative integer m]. In Eq. (2), $K_m(\mu R)$ is then a series of μR , where the contribution to the first-order term is only from $m = \pm l$ and $m = -1 \pm l$, which illustrates the coupling of the adjacent order resulting from the transverse projection of momentum [38]. The sign difference in Eq. (9) shows the complementary stability between the $l = 0$ beam (plus sign) and the $l = 1$ beam (minus sign).

Equation (9) shows the dependence of the acoustic contrast factor on the beam parameters (β and l) and material parameters (λ and κ). We present the multiple parameter dependence in the stability diagram in Fig. 4, where the β value for the transition $\Phi_l(\beta) = 0$, denoted by β_l , is illustrated by the colormap. The two transition limits of $\beta_l = 0^\circ$ (at $f_1/f_2 = 3/2$) and $\beta_l = 90^\circ$ (at $f_1/f_2 = -3(1+l)/4$) divide the stability diagram into four regimes for four types of trapping (Table II). When varying the conical angle β over the whole 90° range, the trapping is preserved or reversed for materials in which the density contrast is relatively small (regimes I and II) or large (regimes III and IV). Note that, in regime IV (or III), there always exists $\beta_1 \leq \beta \leq \beta_0$ for the particle to be trapped at (or be repulsed away from) both the central pressure maximum of axisymmetric beams and minimum of vortex beams, while particles in regimes I and II are always trapped by one beam and repulsed by the other (Table II).

The four cases calculated in Fig. 3 respectively fall into the four regimes in Fig. 4, with the contrast factors given by Eq. (4), where the bulk modulus is $K_0 = \rho_0 c_0^2$ for background medium, $K = \rho c^2$ for a droplet, and $K = \rho[c_L^2 - (4/3)c_T^2]$ for an elastic sphere, with c_L and c_T being the

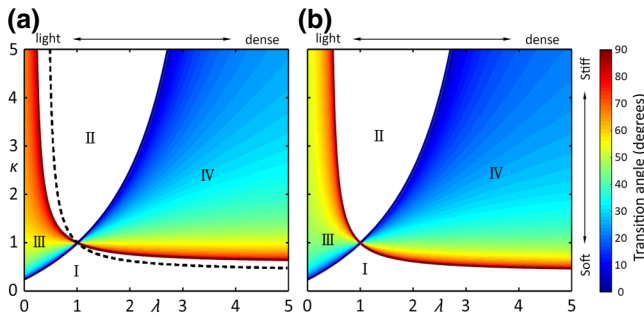


FIG. 4. Stability diagram for (a) $l = 0$ and (b) $l = 1$ beams, illustrating the transition of trapping at a critical paraxiality parameter β_l (colorbar) in the parameter space of density ratio λ and bulk modulus ratio κ [see Eq. (5)]. See Table II about the stability feature of the four regimes I–IV divided by the two boundaries, $f_1/f_2 = 3/2$ (increasing curve) and $f_1/f_2 = -3(1+l)/4$ (descending curve), following from Eq. (9). For comparison, the dashed line in (a) illustrates the boundary of the transition for plane standing-wave trapping, $f_1/f_2 = -3/2$, overlapped with the $\beta = 90^\circ$ standing-wave boundary in (b).

TABLE II. Stability transition for the four regimes in Fig. 4.

	I	II	III	IV
Axisymmetric beam ($l = 0$)	Stable for all β	Unstable for all β	Stable for $\beta > \beta_l$	Stable for $\beta < \beta_l$
Vortex beam ($l = 1$)	Unstable for all β	Stable for all β	Stable for $\beta < \beta_l$	Stable for $\beta > \beta_l$

longitudinal and transverse wave velocities of the material, respectively. For a hollow elastic shell with an inner-to-outer radius ratio b/a , the density ρ and bulk modulus K should be replaced by the effective mass density and effective bulk modulus:

$$\rho_{\text{eff}} = [1 - (b/a)^3]\rho,$$

$$K_{\text{eff}} = \frac{[1 - (b/a)^3]K}{1 + (b/a)^3[0.75(c_L/c_T)^2 - 1]}, \quad (11)$$

which follow from s_n in the Appendix and agrees with [39, 40] in more complex situations.

Importantly, dense and stiff particles (regime IV in Fig. 4) can now be trapped by the axisymmetric beam with a small paraxiality parameter β , as well as by vortex beams but with a large paraxiality parameter. This result suggests a new way to realize trapping of a dense and stiff particle in a simple scheme by using a small β axisymmetric beam, instead of using a relatively complex scheme with vortex beams. For a rigid sphere in the dense limit, the trapping is for $\beta < 28^\circ$ using an axisymmetric beam and for $\beta > 24^\circ$ using $l = 1$ vortex beams [$f_1 = 1$ and $f_2 = 1$ in Eq. (4)].

IV. STABLE TRACTOR BEAMS

We implement the stability diagram to seek the stable trapping in situations where the object is pulled toward the beam source [2–4, 14] (namely, a *stable tractor beam*). By using the axisymmetric Bessel beam, the stability diagram Fig. 4(a) implies that the simultaneous trapping and pulling of a Rayleigh particle is favored for relatively stiff and light particles in regime III or relatively soft and dense particles in regimes I and IV, where the trapping can be achieved by using a large paraxiality parameter β that is also favored by momentum projection to pull particles [3].

Consider the $l = 0$ beam; coupling between the scattered monopole and dipole field leads to the axial radiation force $F_z = \pi a^2 (I_0/c_0) Y_z$, with

$$Y_z = \frac{1}{9} (ka)^4 f_2^2 \cos \beta [(1 + 2f_1/f_2)^2 + 2P_2(\cos \beta)], \quad (12)$$

which is Eq. (15) in Ref. [2] and the Legendre function $P_2(\cos \beta) = (3 \cos^2 \beta - 1)/2$. Given the material parameters, the force is negative when β is larger than a critical angle given by $Y_z(\beta) = 0$. The minimum β value is about 55° for particles with material contrast $f_1/f_2 = -1/2$.

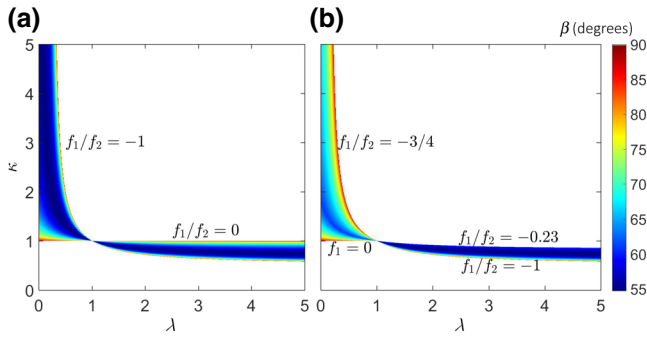


FIG. 5. Diagrams for (a) pulling and (b) simultaneous trapping and pulling of a Rayleigh particle in the parameter space of (λ, κ) , with the colorbar illustrating the minimum paraxiality parameter required for the axisymmetric $l = 0$ Bessel beam. The values of f_1/f_2 on the boundaries are determined by Eqs. (9) and (12).

Larger β fulfills a larger region of negative force in the parameter space of the mass density ratio and bulk modulus ratio. The negative force exists for materials whose contrast is within the regime bounded by $f_1/f_2 = -1$ and $f_1/f_2 = 0$ [Fig. 5(a)].

Regions for simultaneously trapping and pulling a Rayleigh particle are obtained by combining Eqs. (9) and (12) or combining Figs. 4(a) and 5(a) *per se*. The results are shown in Fig. 5(b) with the color plots illustrating the minimum parameter β required. The minimum β is determined by the critical values for pulling in Fig. 5(a)

and for trapping in Fig. 4(a). In the region $\lambda > 1$, for $f_1/f_2 > -3/4$, the β also needs to be less than the critical angle for stable trapping in regime IV of Fig. 4(a). The boundary $f_1/f_2 = -0.23$ in Fig. 5(b) corresponds to the situation when the minimum β angle for pulling equals the maximum β angle for trapping. We hence identify the beam and material parameters for the simultaneous pulling and trapping of a Rayleigh particle.

For other material parameters outside that shown in Fig. 5(b), one would have to use a ka outside the Rayleigh regime to achieve the simultaneous trapping and pulling; see Fig. 6. The results are calculated from the dimensionless forces Y_ρ and Y_z from Eq. (16) in Ref. [17] (with $R = 0$ therein; see also [41]). In the Rayleigh regime (Fig. 6), only the aluminum shell in water is stably pulled by the axisymmetric beam because the parameters lie in the stable pulling region in Fig. 5(b) with the effective mass density ratio $\lambda_{\text{eff}} = 0.31$ and the effective bulk modulus ratio $\kappa_{\text{eff}} = 1.44$ [see Eq. (11)]. For this case, the minimum β required for the trapping is about 65° and that required for pulling is about 56° .

In the practical situation though, one would need to include the correction by thermoviscous absorption. The absorption degrades the negative force [3,21] and consequently increases the minimum β required, as illustrated in Fig. 7 for the simultaneous pulling and trapping of the aluminum shell in water in the parameter space ka and a . The correction to the axial force is dominated by the term [3] $Y_z^{\text{abs}} = Q_{\text{abs}} \cos \beta$, where $\cos \beta$ accounts for the projection of momentum to the propagation axis and Q_{abs}

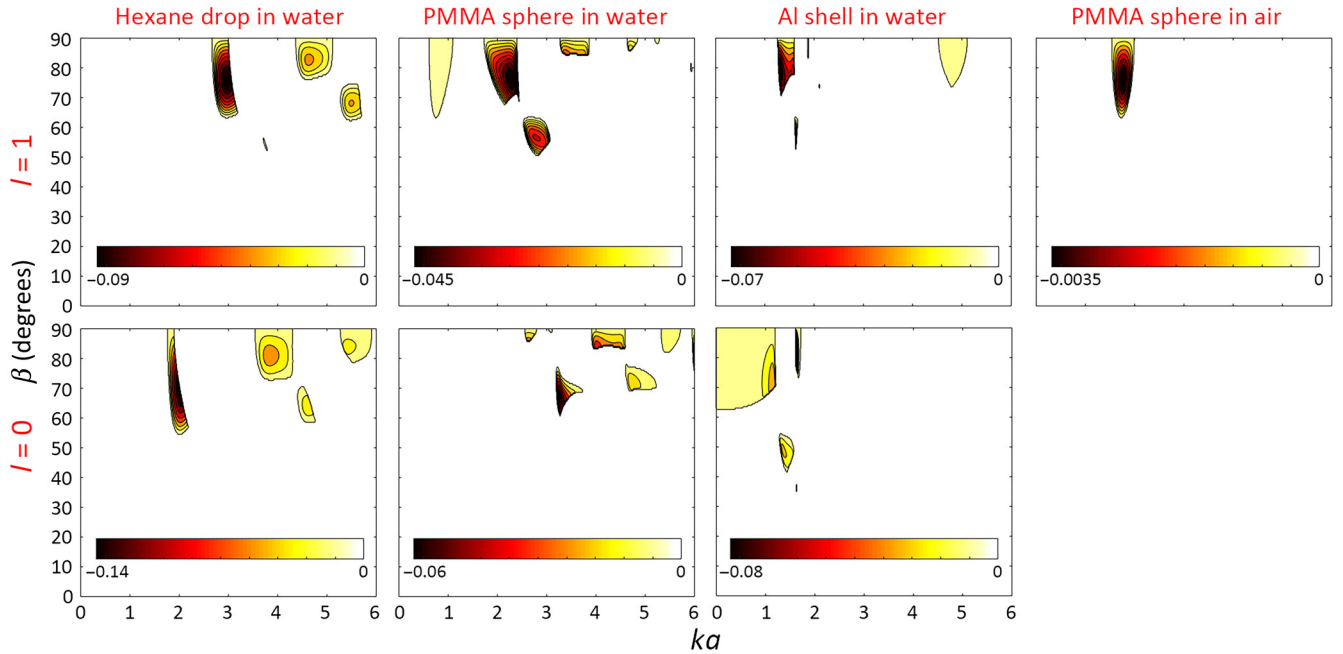


FIG. 6. Contour plots in the parameter space of (ka, β) , where particles are simultaneously trapped and pulled. The results are for $l = 1$ (upper panels) and $l = 0$ (bottom panels). Only the aluminum shell is stably pulled by axisymmetric beam in the Rayleigh regime because the aluminum shell lies in the stable pulling region in Fig. 5 [$(\lambda, \kappa) = (0.31, 1.44)$].

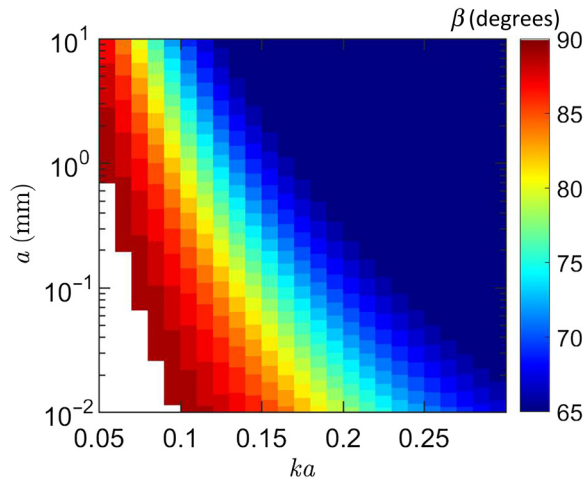


FIG. 7. Minimum β for simultaneous pulling and trapping of an empty aluminum shell centered on the axis of axisymmetric Bessel beams in the parameter space (ka, a) when the loss correction is included. At the small ka and a values, β approaches to 90° (white region).

is the absorption efficiency. For the range of ka examined herein, it is satisfactory to approximate the force experienced by the elastic shell by retaining only the monopole and dipole terms [42]. The range of the ratio of the boundary thickness to the sphere radius, δ/a , in Fig. 7, is from 0.0002 to 0.05, where the ratio

$$\delta/a = \sqrt{2\nu/\omega}/a = (2\nu/ca)^{1/2}/(ka)^{1/2} \quad (13)$$

is a function of a and ka [21] (ν denotes the kinematic viscosity of the surrounding fluid). Following from the $\delta/a \ll 1$ approximation, the absorption efficiency is [3,43]

$$Q_{\text{abs}} \approx 12(ka)^{1/2}(2\nu/ca)^{1/2}[(\lambda - 1)/(1 + 2\lambda)]^2 \cos^2 \beta, \quad (14)$$

which accounts for the viscous power dissipation near the small solid sphere; the loss contribution to the monopole term is neglected [which is satisfactory unless Q_{abs} in Eq. (14) is significantly reduced when β is near 90°]. With these approximations, Fig. 7 demonstrates the existence of a stable tractor beam (i.e., simultaneous pulling and trapping) for a small particle when loss correction is included. The results will guide the experimental realization [44].

V. SUMMARY AND DISCUSSION

In summary, we systematically examine behaviors of acoustic beam trapping when varying the multiple parameters of the beam and materials. Several unusual behaviors are found, such as stable trapping of elastic particles or even a rigid particle by axisymmetric beams of a small paraxiality, reversal of trapping when reducing the paraxiality parameter, trapping of certain particles

by both an axisymmetric beam and vortex beam, and simultaneous trapping and pulling of a Rayleigh particle by axisymmetric beams. We present thorough insight into these behaviors by the Gor'kov potential, features of three-dimensional velocity fields of the sound beams, momentum projection, beam-parameter-dependent acoustic contrast factor, and stability diagram. The trapping is reversed when β is reduced to be smaller than the critical value and when the density contrast is large enough. The results are an approximation for trapping by beams that have a relatively weak focusing or diffracting.

Insights into variation of beam trapping with beam parameters and the seemingly unusual behaviors can drive development of new devices and techniques for simplified and flexible traps. Based on our investigations, we suggest simplified schemes to (a) trap a dense and stiff particle by an axisymmetric beam of a small paraxiality parameter (besides using a vortex beam of a large paraxiality) and (b) simultaneously pull and trap a Rayleigh particle by an ordinary Bessel beam (with the paraxiality parameter large enough). These schemes pave the way toward engineering *simplified* acoustic tweezers and *stable* tractor beams for microparticles by using ordinary beams.

The results in the standing-wave limit ($\beta = 90^\circ$) are applicable to trapping by two orthogonal standing waves [45], where the fields near the nodes and antinodes are approximated by the $l = 0$ and $l = 1$ Bessel-function fields [19]. The trapping criteria are [see Eq. (9)]

$$\begin{aligned} f_1/f_2 &< -3/4 \text{ for trapping at pressure nodes;} \\ f_1/f_2 &> -3/2 \text{ for trapping at pressure antinodes.} \end{aligned} \quad (15)$$

Particles whose parameters are in the regime between these two transitions are trapped or repulsed by both the nodes and antinodes.

On the other hand, trapping conditions for a Rayleigh particle can be simplified by using higher-order beams. For instance, the trapping by an $l = 2$ beam has an acoustic contrast factor [Eq. (9)]

$$\Phi_2(\beta) = 1/8 \sin^2 \beta f_2, \quad (16)$$

which depends on the mass density ratio but not the bulk modulus ratio, where dense (light) particles are repulsed (attracted) and there is no reversal of the trapping when varying the paraxiality parameter β in this case. It is noteworthy that the trapping force by higher-order beams is weaker to precisely trap axially centered Rayleigh particles. Further, the nonconservative radiation force along the axis direction exerted by the $l = 2$ beam on the Rayleigh particle is negligible, which in turn gives more flexibility to manipulate the axial force for particles beyond the Rayleigh regime.

ACKNOWLEDGMENTS

The support of the start-up fund from the University of Mississippi and the fund from Gulf Research Program of the National Academy of Sciences is acknowledged.

APPENDIX: SCATTERING FUNCTIONS FOR DIFFERENT PARTICLES

The scattering functions s_n [37], which are determined by the boundary conditions and material properties, can be calculated by

$$s_n = -\frac{D_n^*}{D_n}, \quad (\text{A1})$$

where D_n is a function of ka and material parameters. It has $|s_n| \leq 1$ and, when losses are negligible, $|s_n| = 1$.

For a rigid sphere [2],

$$D_n = h_n^{(1)'}(x), \quad (\text{A2})$$

where $h_n^{(1)}(x)$ is the first kind of spherical Hankel function with $x = ka$ and $'$ represents the derivative with respect to the argument.

For a fluid sphere [2],

$$D_n = \lambda x j_n(x/\sigma) h_n^{(1)'}(x) - x/\sigma j_n'(x/\sigma) h_n^{(1)}(x), \quad (\text{A3})$$

where $j_n(x)$ is the spherical Bessel function and $\lambda = \rho/\rho_0$ and $\sigma = c/c_0$ are the density ratio and the speed ratio of a particle to the background medium, respectively.

For a solid sphere [46], D_n is the determinant of the 3×3 matrix having the following elements:

$$\begin{aligned} d_{11} &= (z^2/\lambda)h_n^{(1)}(x), \\ d_{12} &= (2N - z^2)j_n(y) - 4yj_n'(y), \\ d_{13} &= 2N[zj_n'(z) - j_n(z)], \\ d_{21} &= -xh_n^{(1)'}(x), \\ d_{22} &= yj_n'(y), \\ d_{23} &= Nj_n(z), \\ d_{31} &= 0, \\ d_{32} &= 2[j_n(y) - yj_n'(y)], \\ d_{33} &= 2zj_n'(z) + [z^2 - 2N + 2]j_n(z), \end{aligned} \quad (\text{A4})$$

where $x = ka$, $y = (c/c_L)x$, $z = (c/c_T)x$, and $N = n(n+1)$.

For a solid shell with outer and inner radius of a and b [46], D_n is the determinant of the 5×5 matrix with the same elements as those for a solid sphere and the remaining elements given by

$$\begin{aligned} d_{14} &= [2N - z^2]n_n(y) - 4yn_n'(y), \\ d_{15} &= 2N[zn_n'(z) - n_n(z)], \end{aligned}$$

$$\begin{aligned} d_{24} &= yn_n'(y), \\ d_{25} &= Nn_n(z), \\ d_{34} &= 2[n_n(y) - yj_n'(y)], \\ d_{35} &= 2zn_n'(z) + [z^2 - 2N + 2]n_n(z), \\ d_{41} &= 0, \\ d_{42} &= [2N - w^2]j_n(u) - 4uj_n'(u), \\ d_{43} &= 2N[wj_n'(w) - j_n(w)], \\ d_{44} &= [2N - w^2]n_n(u) - 4un_n'(u), \\ d_{45} &= 2N[wn_n'(w) - n_n(w)], \\ d_{51} &= 0, \\ d_{52} &= 2[j_n(u) - uj_n'(u)], \\ d_{53} &= 2wj_n'(w) + [w^2 - 2N + 2]j_n(w), \\ d_{54} &= 2[n_n(u) - un_n'(u)], \\ d_{55} &= 2wn_n'(w) + [w^2 - 2N + 2]n_n(w), \end{aligned} \quad (\text{A5})$$

where n_n is the spherical Neumann function, $u = (c/c_L)kb$, and $w = (c/c_T)kb$.

-
- [1] A. Ashkin, J. M. Dziedzic, J. E. Bjorkholm, and Steven Chu, Observation of a single-beam gradient force optical trap for dielectric particles, *Opt. Lett.* **11**, 288 (1986).
 - [2] P. L. Marston, Axial radiation force of a Bessel beam on a sphere and direction reversal of the force, *J. Acoust. Soc. Am.* **120**, 3518 (2006).
 - [3] L. K. Zhang, and P. L. Marston, Geometrical interpretation of negative radiation forces of acoustical Bessel beams on spheres, *Phys. Rev. E* **84**, 035601 (2011).
 - [4] L. K. Zhang, and P. L. Marston, Axial radiation force exerted by general non-diffracting beams, *J. Acoust. Soc. Am.* **131**, EL329 (2012).
 - [5] S. H. Lee, Y. Roichman, and D. G. Grier, Optical solenoid beams, *Opt. Express* **18**, 6988 (2010).
 - [6] J. Chen, J. Ng, Z. F. Lin, and C. T. Chan, Optical pulling force, *Nat. Photonics* **5**, 531 (2011).
 - [7] A. Novitsky, C.-W. Qiu, and H. Wang, Single Gradientless Light Beam Drags Particles as Tractor Beams, *Phys. Rev. Lett.* **107**, 203601 (2011).
 - [8] S. Sukhov, and A. Dogariu, Negative Nonconservative Forces: Optical ‘Tractor Beams’ for Arbitrary Objects, *Phys. Rev. Lett.* **107**, 203602 (2011).
 - [9] N. Wang, J. Chen, S. Y. Liu, and Z. F. Lin, Dynamical and phase-diagram study on stable optical pulling force in Bessel beams, *Phys. Rev. A* **87**, 063812 (2013).
 - [10] O. Brzobohatý, V. Karásek, M. Šiler, L. Chvátal, T. Čižmár, and P. Zemánek, Experimental demonstration of optical transport, sorting and self-arrangement using a ‘tractor beam’, *Nat. Photonics* **7**, 123 (2013).

- [11] V. Shvedov, A. R. Davoyan, C. Hnatovsky, N. Engheta, and W. Krolikowski, A long-range polarization-controlled optical tractor beam, *Nat. Photonics* **8**, 846 (2014).
- [12] S. Xu, C. Qiu, and Z. Liu, Transversally stable acoustic pulling force produced by two crossed plane waves, *Europhys. Lett.* **99**, 44003 (2012).
- [13] C. E. M. Démoré, P. M. Dahl, Z. Yang, P. Glynne-Jones, A. Melzer, S. Cochran, M. P. MacDonald, and G. C. Spalding, Acoustic Tractor Beam, *Phys. Rev. Lett.* **112**, 174302 (2014).
- [14] D. B. Thiessen, L. K. Zhang, and P. L. Marston, Radiation force on spheres in helicoidal Bessel beams modeled using finite elements, *J. Acoust. Soc. Am.* **125**, 2552 (2009).
- [15] D. Baresch, J. L. Thomas, and R. Marchiano, Three-dimensional acoustic radiation force on an arbitrarily located elastic sphere, *J. Acoust. Soc. Am.* **133**, 25 (2013).
- [16] G. T. Silva, J. H. Lopes, and F. G. Mitri, Off-axial acoustic radiation force of repulsor and tractor Bessel beams on a sphere, *IEEE Trans. Ultrason. Ferroelectr. Freq. Control* **60**, 1207 (2013).
- [17] L. K. Zhang, Reversals of Orbital Angular Momentum Transfer and Radiation Torque, *Phys. Rev. Appl.* **10**, 034039 (2018).
- [18] P. L. Marston, Radiation force of a helicoidal Bessel beam on a sphere, *J. Acoust. Soc. Am.* **125**, 3539 (2009).
- [19] L. K. Zhang, and P. L. Marston, Acoustic radiation torque on small objects in viscous fluids and connection with viscous dissipation, *J. Acoust. Soc. Am.* **136**, 2917 (2014).
- [20] P. L. Marston, Viscous contributions to low-frequency scattering, power absorption, radiation force, and radiation torque for spheres in acoustic beams, *Proc. Meet. Acoust.* **19**, 045005 (2013).
- [21] P. L. Marston, and L. K. Zhang, Relationship of scattering phase shifts to special radiation force conditions for spheres in axisymmetric wave-fields, *J. Acoust. Soc. Am.* **141**, 3042 (2017).
- [22] L. P. Gor'kov, On the forces acting on a small particle in an acoustical field in an ideal fluid, *Sov. Phys. Dokl.* **6**, 773 (1962).
- [23] P. L. Marston, and D. B. Thiessen, Manipulation of fluid objects with acoustic radiation pressure, *Ann. N.Y. Acad. Sci.* **1027**, 414 (2006).
- [24] F. Petersson, A. Nilsson, C. Holm, H. Jonsson, and T. Laurell, Continuous separation of lipid particles from erythrocytes by means of laminar flow and acoustic standing wave forces, *Lab Chip* **5**, 20 (2005).
- [25] J. Wu, Acoustical tweezers, *J. Acoust. Soc. Am.* **89**, 2140 (1991).
- [26] X. C. Chen, and R. E. Apfel, Radiation force on a spherical object in an axisymmetric wave field and its application to the calibration of high-frequency transducers, *J. Acoust. Soc. Am.* **99**, 713 (1996).
- [27] J. Lee, S. Y. Teh, A. Lee, H. H. Kim, C. Lee, and K. K. Shung, Single Beam Acoustic Trapping, *Appl. Phys. Lett.* **95**, 073701 (2009).
- [28] Y. Choe, J. W. Kim, K. K. Shung, and E. S. Kim, Microparticle Trapping in an Ultrasonic Bessel Beam, *Appl. Phys. Lett.* **99**, 233704 (2011).
- [29] S. T. Kang, and C. K. Yeh, Potential-well model in acoustic tweezers, *IEEE Trans. Ultrason. Ferroelectr. Freq. Control* **57**, 1451 (2010).
- [30] A. Marzo, S. A. Seah, B. W. Drinkwater, D. R. Sahoo, B. Long, and S. Subramanian, Holographic acoustic elements for manipulation of levitated objects, *Nat. Commun.* **6**, 8661 (2015).
- [31] D. Baresch, J.-L. Thomas, and R. Marchiano, Observation of a Single-beam Gradient Force Acoustical Trap for Elastic Particles: Acoustical Tweezers, *Phys. Rev. Lett.* **116**, 024301 (2016).
- [32] K. Melde, A. G. Mark, T. Qiu, and P. Fischer, Holograms for acoustics, *Nature* **537**, 518 (2016).
- [33] A. Marzo, A. Ghobrial, L. Cox, M. Caleap, A. Croxford, and B. W. Drinkwater, Realization of Compact Tractor Beams using Acoustic Delay-lines, *App. Phys. Lett.* **110**, 014102 (2017).
- [34] A. Marzo, M. Caleap, and B. W. Drinkwater, Acoustic Virtual Vortices with Tunable Orbital Angular Momentum for Trapping of Mie Particles, *Phys. Rev. Lett.* **120**, 044301 (2018).
- [35] G. T. Silva, Acoustic radiation force and torque on an absorbing compressible particle in an inviscid fluid, *J. Acoust. Soc. Am.* **136**, 2405 (2014).
- [36] C. R. P. Courtney, B. W. Drinkwater, C. E. M. Demore, S. Cochran, A. Grinenko, and P. D. Wilcox, Dexterous Manipulation of Microparticles using Bessel-function Acoustic Pressure Fields, *Appl. Phys. Lett.* **102**, 123508 (2013).
- [37] L. K. Zhang, and P. L. Marston, Acoustic radiation force expressed using complex phase shifts and momentum-transfer cross sections, *J. Acoust. Soc. Am.* **140**, EL178 (2016).
- [38] L. K. Zhang, From acoustic radiation pressure to three-dimensional acoustic radiation forces, *J. Acoust. Soc. Am.* **144**, 443 (2018).
- [39] X. M. Zhou, G. K. Hu, and T. J. Lu, Elastic wave transparency of a solid sphere coated with metamaterials, *Phys. Rev. B* **77**, 024101 (2008).
- [40] J. P. Leo-Neto, J. H. Lopes, and G. T. Silva, Core-shell Particles that are Unresponsive to Acoustic Radiation Force, *Phys. Rev. Appl.* **6**, 024025 (2016).
- [41] L. K. Zhang, A general theory of arbitrary bessel beam scattering and interactions with a sphere, *J. Acoust. Soc. Am.* **143**, 2796 (2018).
- [42] P. L. Marston, Phase-shift derivation of expansions for material and frequency dependence of progressive-wave radiation forces and backscattering by spheres, *J. Acoust. Soc. Am.* **145**, EL39 (2019).
- [43] P. L. Marston, and L. K. Zhang, Unphysical consequences of negative absorbed power in linear passive scattering: Implications for radiation force and torque, *J. Acoust. Soc. Am.* **139**, 3139 (2016).
- [44] A streaming flow generated by the attenuation of the propagating beam in a fluid is beyond our consideration, though there are situations where the force due to streaming in water may be neglected during the measurement [21].
- [45] J. Shi, D. Ahmed, X. Mao, S.-C. S. Lin, A. Lawit, and T. J. Huang, Acoustic tweezers: Patterning cells and microparticles using standing surface acoustic waves (ssaw), *Lab Chip* **9**, 2890 (2009).
- [46] P. L. Marston, Acoustic beam scattering and excitation of sphere resonance: Bessel beam example, *J. Acoust. Soc. Am.* **122**, 247 (2007).